DOI: 10.1002/chem.200601190

From Molecule to Bulk Material: Optical Properties of Hydrogen-Bonded Dimers $[C_{12}H_{12}N_4O_2AgPF_6]_2$ and $[C_{28}H_{28}N_6O_3AgPF_6]_2$ Depend on the Arrangement of the Oxime Moieties

Wen-Dan Cheng,* Dong-Sheng Wu, Juan Shen, Shu-Ping Huang, Zhi Xie, Hao Zhang, and Ya-Jing Gong[a]

Abstract: The dependence of the optical properties of $[C_{12}H_{12}N_4O_2AgPF_6]_2$ (dimer-1) and $[C_{28}H_{28}N_6O_3AgPF_6]_2$ (dimer-2) on the arrangement of the oxime moieties in the molecule and in bulk crystals was investigated by means of time-dependent density functional theory. Dimer-1 with simple pyridine oxime ligands and a wavy arrangement has a smaller dipole moment and larger transition energy between the two states, and thus smaller third-order polarizabilities and two-photon absorption cross sections. Dimer-2 with extended pyridine oxime ligands and a ladder arrangement has a larger dipole moment and smaller transition energy between the two states, and thus larger third-order polarizabilities and two-photon absorption cross sections. The lowest energy absorption band is red-shifted for dimer-2 as compared with dimer-1, due to more pronounced π–π delocalization interactions and weaker hydrogen bonding in dimer-2. The electronic absorption spectra, frequency-dependent third-order polarizabilities, and two-photon absorption cross sections involve significant contributions from charge transfers from π/π* orbitals of the pyridine oxime ligands but no contribution from PF_6^- ions or H_2O molecules in the wavelength range studied for the monomers and dimers of the $C_{12}H_{12}N_4O_2AgPF_6$ and $C_{28}H_{28}N_6O_3AgPF_6$ molecules. The third-order susceptibilities and two-photon absorption coefficients of bulk solids were estimated on the basis of the optical properties of the corresponding dimers, and the bulk material constructed from dimer-2 has the larger optical parameters of the two.

Keywords: density functional calculations · hydrogen bonds · nonlinear optics · oxime ligands · silver

Introduction

Molecules and molecular clusters are building blocks of solid materials, and the development of new materials with a variety of properties, functions, and applications is an aim of materials scientists and technologists. The physical properties of the materials depend on their molecular components and the manner in which they are arranged and linked in the crystalline state. The successful design of new materials with distinctive properties by the crystal-engineering method[1–5] is based upon detailed understandings of noncovalent interactions and optimal arrangement of molecular components into extended solid-state architectures.[6,7] Accordingly, before we determine spectral properties of the material, such as supersusceptibility and two-photon absorption spectra, we must understand the structure of a single molecule, as well as the interaction strengths and relative orientations among the molecules in a material. We are especially interested in the properties of nonlinear polarizability and two-photon absorption, because materials with these properties have a number of potential applications such as optical power limitation,[8,9] two-photon laser scanning microscopy,[10–12] and high-density optical data storage.[13–14] For a solid constructed by noncovalent interaction among molecules, the spectral properties of the solid state simply arise from the single-molecule structure and the manner in which the molecules are packed. Therefore, investigating the optical properties of molecular clusters is a prerequisite for studies on the optical properties of materials.

[a] Prof. W.-D. Cheng, Dr. D.-S. Wu, Dr. J. Shen, Dr. S.-P. Huang, Dr. Z. Xie, H. Zhang, Y.-J. Gong
State Key Laboratory of Structural Chemistry
Fujian Institute of Research on the Structure of Matter
The Chinese Academy of Sciences
Fuzhou, Fujian 350002 (P. R. China)
Fax: (+86) 0591-8371-4946
E-mail: cwd@ms.fjirsm.ac.cn

Supporting information for this article is available on the WWW under http://www.chemeurj.org/ or from the author.

A good example of crystal engineering for predesigned materials properties is the use of an intermolecular connector that can generate infinite architectures through complementary hydrogen bonding of oxime groups in a dimeric $R_2^2(6)$ motif.[15,16] Simple and extended pyridine oxime ligands were employed in the design of silver(I)-containing hydrogen-bonded networks in which the geometry encoded in the coordination complex is propagated into low-dimensional architectures through intermolecular oxime–oxime hydrogen bonds, and supramolecular interaction based on oxime–oxime interaction is not substantially disrupted despite extensive ligand modifications.[17,18] These hydrogen-bonded molecular clusters give us the opportunity to study the influences of hydrogen-bonding interactions, single-molecule size, and the relative arrangements of molecules on the optical spectra of molecular clusters. Furthermore, optical properties of the bulk materials are determined by those of the molecular clusters. It is thus possible to design molecular-cluster-based bulk materials with a given optical property when the origin of the optical properties of hydrogen-bonded molecular cluster has been elucidated.

Computational Methods

The single-point calculations of ground-state wave functions and energies were based on DFT with the B3LYP hybrid functional including exchange-correlation interactions[19] and 6-31* basis set, and the natures of electronic excited states were computed by using time-dependent DFT (TDDFT) at the B3LYP/3-21G* level[20–22] with the Gaussian 03 program suite[23] for the monomers and dimers of $C_{12}H_{12}N_4O_2AgPF_6$ and $C_{28}H_{28}N_6O_3AgPF_6$. The effects of basis sets on calculations of NLO polarizability by using ab initio or DFT calculations combined with finite-field methods were taken into account in previous work.[24,25] In the SOS calculations of NLO polarizability, influence of basis sets has also been discussed.[26] Here, we selected the 3-21G* basis set for the excited states and SOS calculations, considering the balance between accuracy and available resources, to make systematic comparisons between the large $[C_{12}H_{12}N_4O_2AgPF_6]_2$ and $[C_{28}H_{28}N_6O_3AgPF_6]_2$ systems. The binding energies or hydrogen-bond energies between the monomers were obtained in terms of the calculated single-point energies of monomers and dimers. In the TDB3LYP/3-21* excited-state calculations, the molecular orbitals for correlation ranged from orbital 48 to 298 (95 to 596) for the monomer (dimer) of $C_{12}H_{12}N_4O_2AgPF_6$, and from orbital 67 to 501 (133 to 1002) for the monomer (dimer) of $C_{28}H_{28}N_6O_3AgPF_6$. Iterations of excited states were continued until the changes in energies of states were no more than 10^{-7} a.u. between iterations, and convergences of 60 excitation states were obtained in the calculations. The third-order polarizabilities for three optical processes were calculated by sum-over-states (SOS) perturbation theory,[27–30] and the inputs of the SOS method were the results calculated by the TDB3LYP/3-21G* method. The frequency dependence of two-photon absorption (TPA) cross sections were obtained by using their relationship with the imaginary part of the third-order polarizability in the degenerate four-wave mixing optical process.[31–33] The geometries used in our calculations were taken from X-ray crystallographic data.[17,18]

Cartesian coordinates of the monomers and dimers of $C_{12}H_{12}N_4O_2AgPF_6$ and $C_{28}H_{28}N_6O_3AgPF_6$ molecules are listed in Tables S1–S4 in the Supporting Information, and frontier molecular orbitals involved in charge-transfer processes are depicted in Figures S1–S3 in the Supporting Information.

Results and Discussion

Supramolecular interactions of dimers: Figure 1a and b show the configurations of $[C_{12}H_{12}N_4O_2AgPF_6]_2$ (dimer-1)

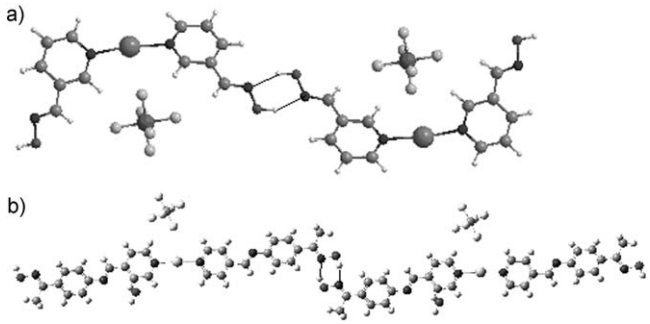

Figure 1. Structures of a) dimer-1 and b) dimer-2.

and $[C_{28}H_{28}N_6O_3AgPF_6]_2$ (dimer-2), respectively.[17,18] The two oxime moieties (−C(R)=NOH) of monomeric $C_{12}H_{12}N_4O_2AgPF_6$ (monomer-1) exist in a *cis* orientation, and this configuration results in the wavy arrangement in the self-complementary oxime–oxime hydrogen-bonded dimer-1. In contrast, dimer-2 has a ladder arrangement resulting from the *trans* arrangement of the terminal oxime moieties in monomeric $C_{28}H_{28}N_6O_3AgPF_6$ (monomer-2). The *cis* and *trans* orientations of the two oxime moieties in the monomer result in different dipole interactions between the monomers in the dimers. For dimer-1, dipole interactions between the monomers cancel each other and bring about a decrease in dipole moment. For dimer-2, enhancement of dipole interactions between the monomers increases the dipole moment. These considerations are corroborated by the calculated dipole moments of monomers and dimers at the B3LYP/6-31* level (Table 1). The dipole moment of

Table 1. Calculated (B3LYP/6-31*) binding energies, dipole moments, and hydrogen-bond energies of dimers **1** and **2**.

Dimer	E_b [eV]	μ [D]	O−H···N [Å]	O−H···N [°]	E_{hb} [kcal mol^{-1}]
1	−0.8357	0.007 (6.381[a])	2.816, 2.816	151.0, 151.0	−9.636
2	−0.7416	27.373 (13.673[a])	2.748, 2.731	160.1, 148.4	−8.551

[a] Dipole moment of monomer.

dimer-1 is about zero, and that of dimer-2 is about twice that of monomer-2. Furthermore, the relative strengths of supramolecular interaction of the hydrogen-bonded dimers can be assessed in terms of electronic binding energies E_b computed for dimers formed by complementary oxime–oxime hydrogen bonding. We define E_b as the difference in SCF energies of dimer and monomers ($E_b = E_{dimer} - 2E_{mono}$) and hydrogen-bond energy ($E_{hb} = {}^1/_2 E_b$). Here the binding energy E_b is the contributions from all types of intermolecular interaction energies within the B3LYP model, such as

charge transfer, electron correlation and exchange, and electrostatic interaction energies. Table 1 lists the calculated O–H···N bond energies and hydrogen bond distances and angles. The oxime–oxime O–H···N bond energies are −9.636 and −8.551 kcal mol^{-1} for dimers-1 and -2, respectively, that is, they are very close. These findings show that the oxime–oxime supramolecular interaction is not substantially disrupted despite the enhanced dipole moment and extensive ligand modifications that increase the aromatic content in dimer-2.

Electronic absorption spectra: Before discussing the absorption spectra of dimers-1 and -2, we need to know the nature of the excited states of the hydrogen-bonded dimers. Accordingly, the transition energies, transition moments, and oscillator strengths of 60 excited states were calculated at the TDB3LYP/3-21G* level for the dimers and their corresponding monomers. Table 2 lists the calculated transition dipole moments in the *x*, *y*, and *z* directions for the ground and important excited states. The electric dipole transition is allowed in the *x* and *y* directions, and the transition moments perpendicular to the molecular plane (*z* direction) are near to zero. These calculated results describe the charge-transfer behavior in the molecular plane. Figure 2 shows the relationships between oscillator strength and absorption wavelength for 60 excited states. Two facts can be

Table 2. Calculated transition energies, moments, and oscillator strengths of important excited states.

State	*E* [eV]	Dipole moment [D]			Oscillator strength
		x	*y*	*z*	
dimer-1					
S1	4.1211	1.3770	−0.9642	0.0913	0.0443
S2	4.1307	0.0107	−0.0079	0.0008	0.0000
S5	4.3055	2.7232	−2.7273	0.4858	0.2463
S15	4.4217	−0.2913	−2.5654	−0.2893	0.1132
S45	4.8479	4.3697	−1.5511	0.1093	0.3954
S47	4.9205	4.4396	−1.2179	0.1431	0.3958
monomer-1					
S1	4.3421	0.0140	0.6302	0.0003	0.0065
S2	4.3431	−0.6932	−0.0419	0.3884	0.0104
S4	4.3450	0.0170	−2.4093	−0.0137	0.0956
S16	5.0201	−3.6645	−0.0015	0.2534	0.2568
S21	5.0639	0.0048	−3.0956	0.0000	0.1840
S44	5.7895	−2.8618	0.0003	0.0366	0.1798
dimer-2					
S1	2.5864	0.0379	−0.0353	−0.0056	0.0000
S18	3.0162	5.3321	0.4698	0.0562	0.7076
S27	3.2092	−4.8608	−0.9482	0.0125	0.2984
S30	3.2475	−3.5916	−0.5148	0.0107	0.1621
S43	3.7380	−2.0293	−0.0353	0.2191	0.0591
S46	3.8235	−2.2118	−0.2125	−0.3432	0.0737
monomer-2					
S1	2.6544	−0.0275	0.0412	0.0043	0.0000
S7	3.0437	7.3749	−0.0056	0.1482	0.6279
S8	3.1350	−3.4470	−0.2384	−0.0086	0.1419
S9	3.2387	−3.8028	−0.2384	−0.0168	0.1783
S47	4.5534	−6.9890	−0.2468	0.0346	0.8444
S48	4.5989	−2.5560	−0.1365	−0.0641	0.1143

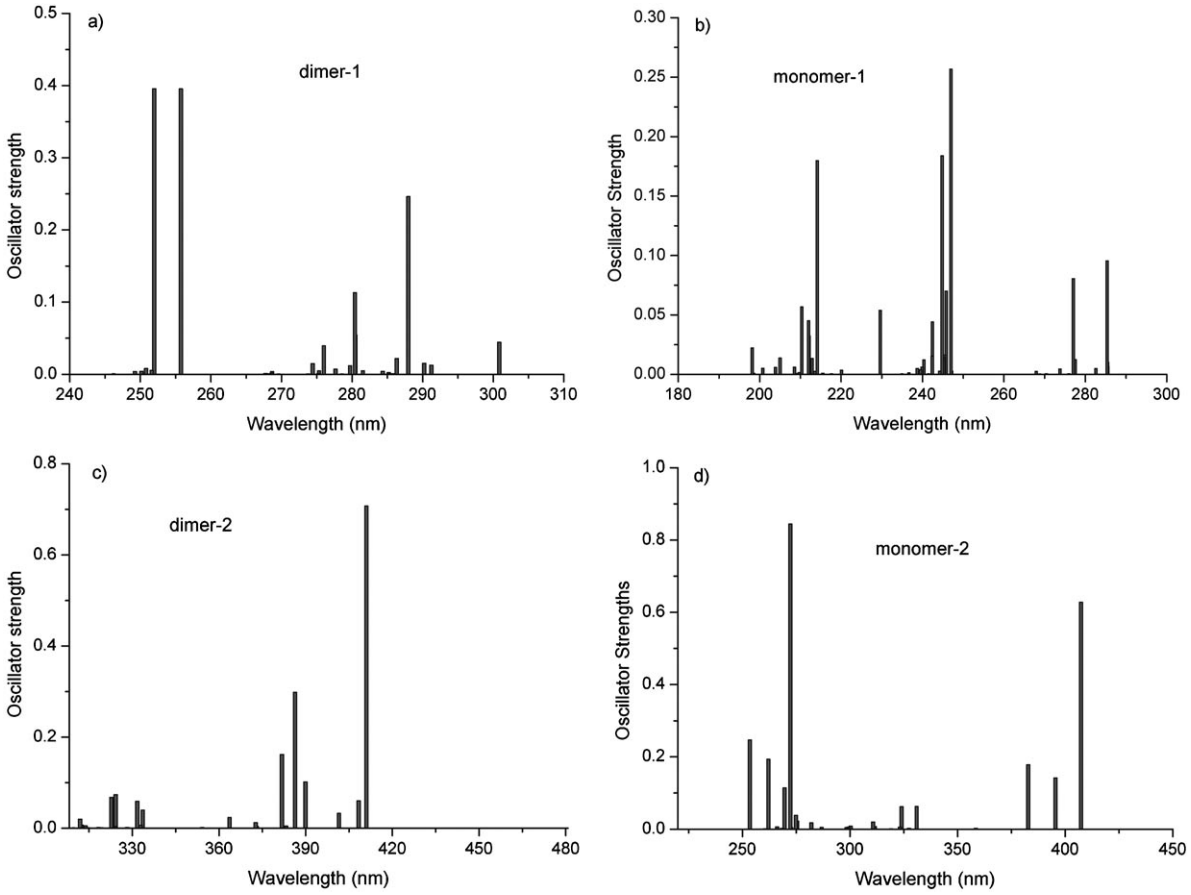

Figure 2. Electronic absorption peaks calculated at the TDB3LYP/3-21* level.

found from the plots in Figure 2. First, the absorption band at lowest energy is red-shifted for dimer-2 compared to dimer-1. This is because elongated (pyridylmethylene) aminoacetophenone oxime ligands lead to a significant increase in π/π delocalization interactions in dimer-2 and the hydrogen-bonding interactions are weaker in dimer-2 than in dimer-1. Second, the lowest energy absorption is red-shifted for each dimer as compared with the corresponding monomer. This results from the supramolecular interaction between the monomers, which decreases the excitation energies of the dimers.

Now, we assign the absorption bands. For dimer-1, the three strong absorption peaks corresponding to excited states S5, S45, and S47 are mostly contributions from charge transfer from the hydrogen-bond donor of the oxime group to pyridine ring acceptors. For example, S5 of dimer-1 is mostly constructed from the configuration of (HOMO$-3\rightarrow$ LUMO$+1$), where the HOMO-3 is formed by the same-phase orbitals between oxime–oxime and π-bonding orbitals of pyridine, and the LUMO$+1$ is formed by the different-phase orbitals between the oxime–oxime and π-antibonding orbitals, as shown in Figure 3a and b. For dimer-2, the three strong absorption peaks corresponding to states S18, S27, and S30 are mostly contributions from charge transfer from one monomer to the other. For instance, S18 of dimer-2 is mainly constructed from the configuration (HOMO$-8\rightarrow$ LUMO), where HOMO-8 is formed by the neighboring ring orbitals of two monomers, and LUMO is formed by only one monomer orbital. Figure 3c d show plots of these two orbitals of dimer-2. From the above analysis, we can conclude that the electronic absorption at low energy significantly arises from charge transfers from π–π^* orbitals of pyridine oxime ligands, and there is no contribution from PF_6^- ions and H_2O molecules in dimers.

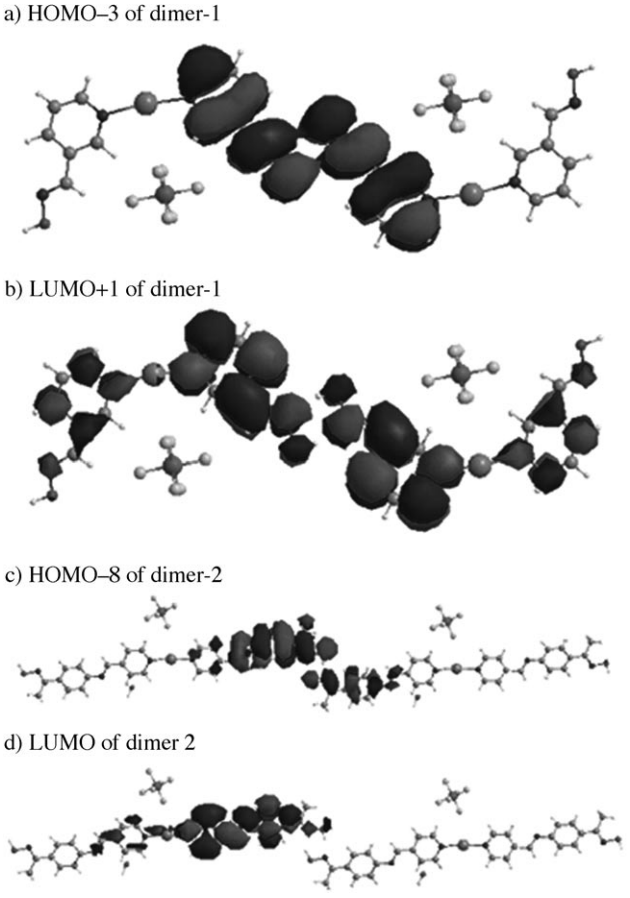

Figure 3. Calculated molecular orbital surface in the ground state.

Third-order polarizability spectra: Frequency-dependent third-order polarizabilities in the ground state were calculated for three optical processes—third-harmonic generation (THG), electric field-induced second-harmonic generation (EFISHG), and degenerate four-wave mixing (DFWM)[27,28]—and plotted in Figure 4. In the static case when the input photon energy is zero, the values of all three processes are the same for each monomer and each dimer. Furthermore, in the dynamic case when the input energy is 0.80 eV, the THG process has a large preresonant character and the DFWM process has a small variation in the studied frequency region. By comparison of Figure 4a and b, we find that the third-order polarizabilities of monomer-2 are larger than those of monomer-1 by about one magnitude. The reasons are: 1) the *trans* arrangement of two oxime moieties in monomer-2 has a lower symmetry than the *cis* arrangement in monomer-1, and this leads to larger dipole moments and transition moments of monomer-2; 2) extended π-electron delocalization results in small transition energies from ground to excited states for monomer-2. This is also evident from the transition moments and energies listed in Table 2. In the context of SOS, third-order polarizability is direct proportional to transition moment and inversely proportional to transition energy. Accordingly, larger third-order polarizabilities of monomer-2 originate from the two aforementioned factors.

The third-order polarizabilities of dimer-1 are about one-half those of the corresponding monomer; however, the third-order polarizabilities of dimer-2 are larger than those of the corresponding monomer by about one order of magnitude. Accordingly, the third-order polarizabilities of dimer-2 are about two orders of magnitude larger than those of dimer-1. Although the binding energies of two monomers or oxime–oxime hydrogen-bonding energies influence the third-order polarizabilities of the two dimers (generally, a stronger supramolecular interaction means a smaller polarizability[26]), much greater differences between the third-order polarizabilities of the two dimers arise from the arrangements of the two oxime moieties of the monomer and the manner of oxime–oxime connection between the two monomers. In dimer-1, the up-down wavy connection of the monomers through the oxime moieties originates from the *cis* arrangement of the two oxime moieties of the monomer, in which the oxime groups at the two terminals of monomer are both down or both up. As mentioned above, this arrangement of dimer-1 results in smaller dipole moments. This is the reason why dimer-1 has smaller third-

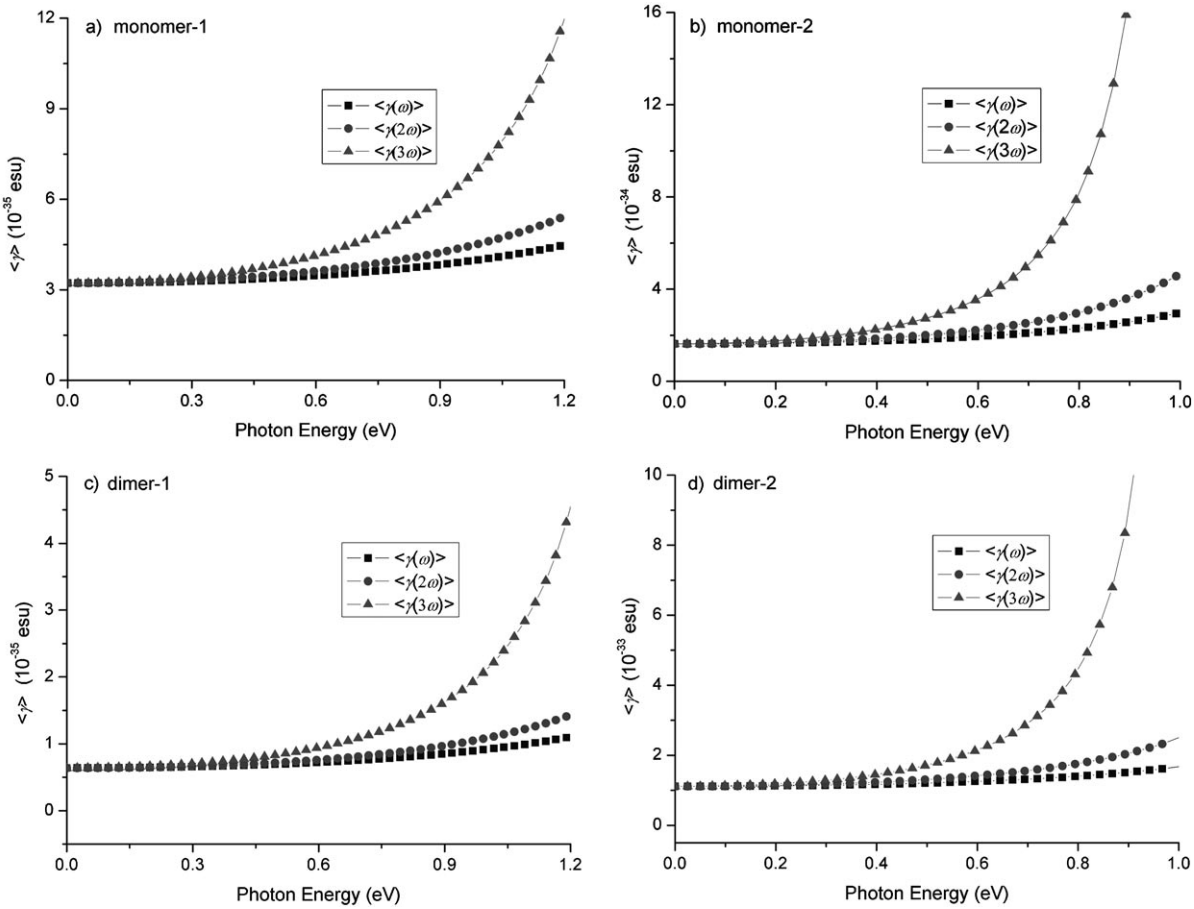

Figure 4. Dynamic third-order polarizabilities calculated at the SOS//TDB3LYP/3-21* level.

order polarizabilities. In dimer-2, the head-to-tail connection of the monomers through the oxime moieties arises from the *trans* arrangement of the two oxime moieties of the monomer, in which one oxime group at one terminal of monomer is up and the other at the other terminal is down (as shown in Figure 1). This arrangement results in the ladder configuration of dimer-2 and results in a large dipole moment. This is the reason why dimer-2 has larger third-order polarizabilities.

Now we investigate the relationship between the third-order polarizability and state natures, and determine which states have the larger contributions to the third-order polarizability. Figure 5 shows the plots of the calculated third-order polarizabilities γ_v, which are the largest components contributing to average polarizability $\langle\gamma(3\omega)\rangle$ in the THG optical process for dimer-1 and dimer-2. Convergences toward stabilization are found after summation over about 25 and 48 states for dimer-1 and dimer-2, respectively. For example, the obtained value of $\gamma_v(3\omega)$ after summation over 20 states is about 90% of $\gamma_v(3\omega)$ after summation over 60 states for dimer-1. Furthermore, it is found from Figure 5 that states S8 and S15 have contributions of 25 and 28% to the $\gamma_v(3\omega)$ value for dimer-1, and states S18 and S23 have contributions of 40 and 36% to the $\gamma_v(3\omega)$ value for dimer-2.[34] States S8 and S15 are mostly constructed by the configurations of $0.3434\,(MO_{241}\rightarrow MO_{245})+0.3053\,(MO_{242}\rightarrow MO_{245})$, and $0.3647\,(MO_{243}\rightarrow MO_{247})+0.3679\,(MO_{243}\rightarrow MO_{248})$, respectively. Figure S1 in the Supporting Information gives plots of these molecular orbitals, and shows the charge transfers from bonding to antibonding orbitals of pyridine oxime ligands in dimer-1. States S18 and S23 of dimer-2 are mostly constructed by the configurations of $0.5401\,(MO_{370}\rightarrow MO_{379})$ and $0.6488\,(MO_{372}\rightarrow MO_{379})$, respectively. Figure S2 in the Supporting Information shows that the occupied orbital ($HOMO-8=MO_{370}$) has the most contributions from the neighboring pyridine oxime ligand group orbitals between the two monomers, and MO_{372} ($HOMO-6$) has contributions from the pyridine oxime ligand orbitals of one half of a monomer. These plots tell us that the charge transfers take place between the two monomers or within one monomer. By comparison of Figures S1 and S2 in the Supporting Information, we find that the orbital charge distributions are highly symmetric in dimer-1 and lay particular stress on the monomer in dimer-2. These findings again provide evidence that dimer-1 has a smaller dipole moment which results in smaller third-order polarizabilities, while dimer-2 has a larger dipole moment that results in larger third-order polarizabilities.

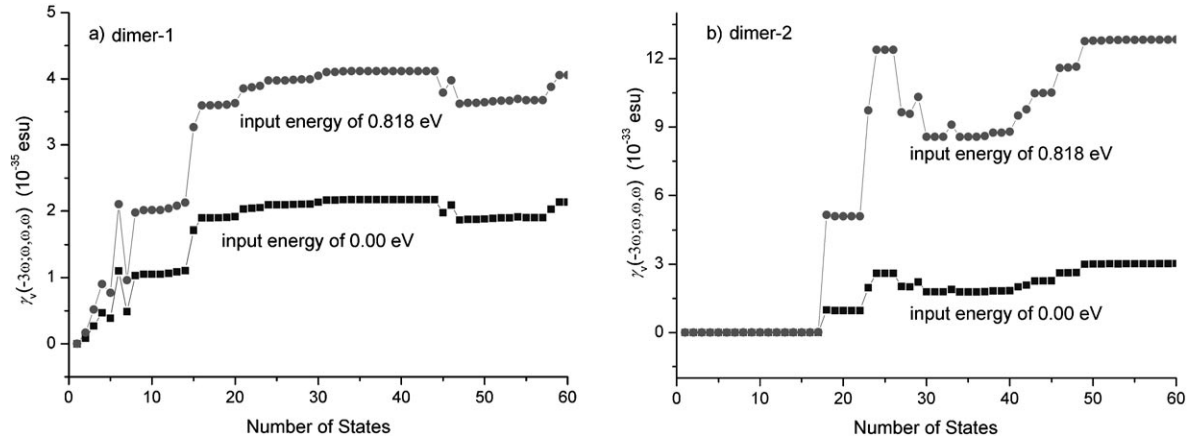

Figure 5. Plots of third-order polarizability in the THG process versus number of states, based on results calculated at the SOS//TDB3LYP/3-21* level.

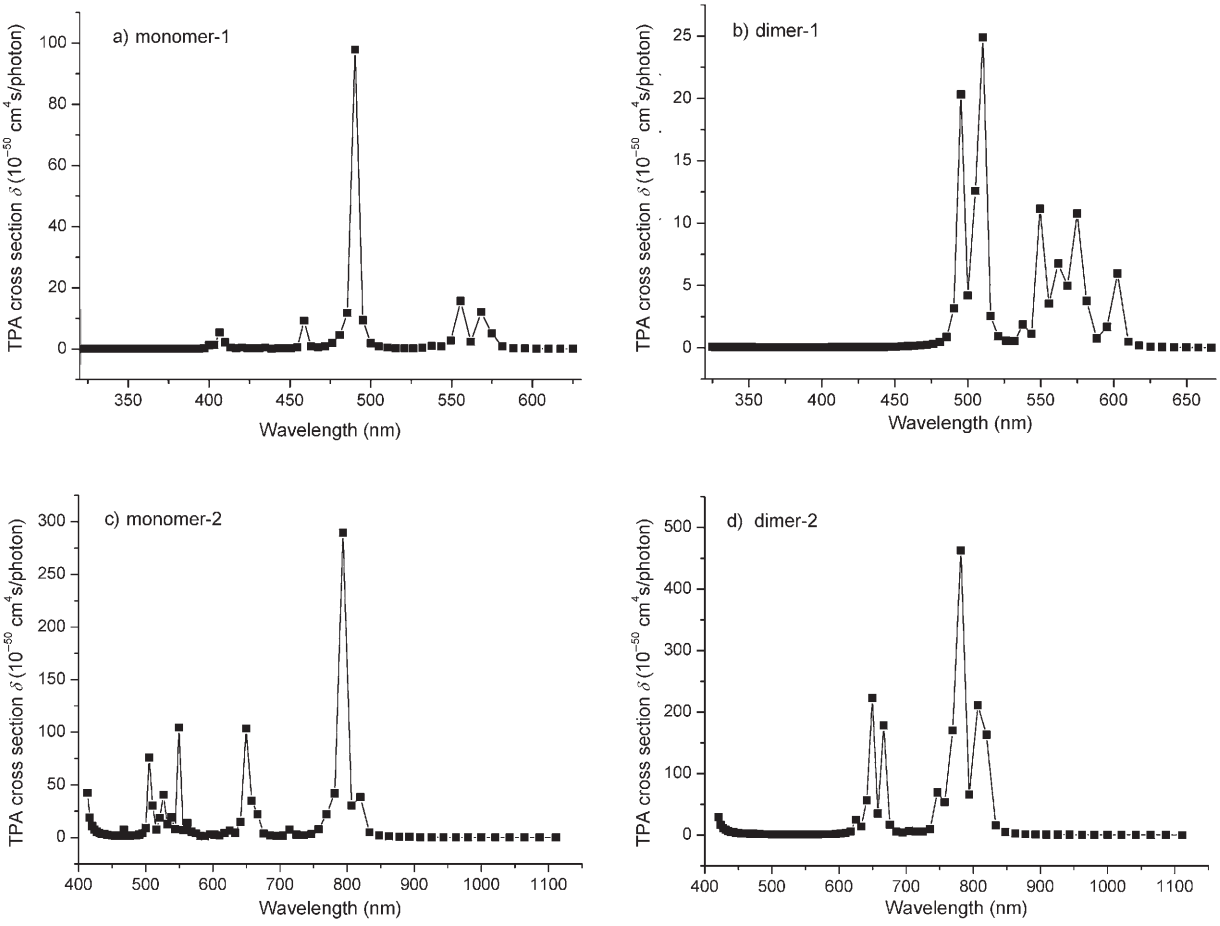

Figure 6. Wavelength-dependent two-photon absorption cross section $\langle\delta(\omega)\rangle$ calculated at the SOS//TDB3LYP/3-21* level.

Two-photon absorption cross sections: The calculated wavelength-dependent TPA cross sections $\langle\delta(\omega)\rangle$ (average of the $\delta(\omega)$ values) of the investigated monomers and dimers are plotted in Figure 6. The largest average resonant TPA values $\langle\delta\rangle$ of dimer-2 and monomer-2 are red-shifted compared with dimer-1 and monomer-1. The largest $\langle\delta\rangle$ values of dimer-1 and monomer-1 are located at about 510 and 490 nm, and those of the dimer-2 and monomer-2 at about 780 and 790 nm, respectively. Dimer-2 has the largest TPA $\langle\delta\rangle$ value of 4.63×10^{-48} cm^4 s photon^{-1} among the investigated species.

Furthermore, in our search for the origin of the large TPA cross sections $\delta(\omega)$ of the dimers and monomers, we found that the $\delta(\omega)$ value only depends on the imaginary

part of third-order polarizability Im$\gamma(-\omega;\omega,\omega,-\omega)$, while the values of refractive indexes and local-field factors are approximated as 1 for vacuum.[31–33] Accordingly, the two-photon states contributing to Im$\gamma(-\omega;\omega,\omega,-\omega)$ also make contributions to the resonant TPA $\delta(\omega)$. Figure 7 presents the plots of Im$\gamma(-\omega;\omega,\omega,-\omega)$ values (related to the TPA cross section of δ) versus two-photon states at the characteristic wavelength (resonant wavelength). It can be seen from Figure 7 that the resonant TPA cross sections of the investigated species all have contributions from one two-photon state. For dimer-1, one electron is promoted from the ground state to state 46 by absorbing two-photon energy, and the transition energy (4.8793 eV) from the ground state to state 46 is equal to the two-photon energy ($2\times$ 2.4396 eV), which results in two-photon resonance absorption at a wavelength of 510 nm (2.430 eV), as shown in Figure 6b. The two-photon state 46 has the greatest contribution from the configurations of $0.5271\,(MO_{242}\rightarrow MO_{250})-0.4395\,(MO_{241}\rightarrow MO_{249})$. For dimer-2, one electron is promoted from the ground state to state 24 by absorbing two-photon energy, and the transition energy (3.1800 eV) from the ground state to state 24 is equal to the two-photon energy (2×1.5900 eV), which results in two-photon resonance absorption at a wavelength of 781 nm (1.588 eV), as shown in Figure 6d. Two-photon state 24 has the greatest contribution from the configurations of $0.5048\,(MO_{370}\rightarrow MO_{380})-0.3817\,(MO_{370}\rightarrow MO_{381})$. By analysis of the molecular orbital plots (shown in Figures S1–S3 in the Supporting Information) involving two-photon absorption, it can be seen that the occupied molecular orbitals (MO_{241} and MO_{242} of dimer-1, MO_{370} of dimer-2) are mostly composed of bonding π orbitals of pyridine oxime ligands, whereas the virtual orbitals (MO_{249} and MO_{250} of dimer-1, MO_{380} and MO_{381} of dimer-2) are composed of antibonding π orbitals of pyridine oxime ligands. Obviously, the two-photon absorptions significantly originate from the electronic transitions from π to π^* orbitals, and have no contribution from PF_6^- anions or H_2O molecules in the studied species.

Third-order nonlinear optical properties of bulk materials: The optical properties of bulk solids can be thought of as being built up from the corresponding properties of the individual molecules or molecular clusters. Accordingly, the third-order optical susceptibilities $\chi^{(3)}$ of bulk materials can be estimated from the average third-order polarizability $\langle\gamma\rangle$, and two-photon absorption coefficients β of bulk materials from TPA cross sections of dimers. The susceptibility $\chi^{(3)}$ is directly related to the average third-order polarizability $\langle\gamma\rangle$ by Equation (1)

$$\chi^{(3)}(-\omega_p;\omega_1,\omega_2,\omega_3) = Nf(\omega_1)f(\omega_2)f(\omega_3)f(\omega_p)\langle\gamma\rangle \quad (1)$$

and the local field factor [Eq. (2)],[35]

$$f(\omega_1) = [n(\omega_i)^2+2]/3 = 1/[1-(4\pi/3)N\alpha(\omega_i)] \quad (2)$$

where $f(\omega_i)$ is at radiation frequency ω_i, N is the dimer number density, and $n(\omega_i)$ and $\alpha(\omega_i)$ are the refractive index and the polarizability, respectively, and can also be obtained by the TDDFT-SOS method. Accordingly, the local field factor $f(\omega_i)$ can be obtained from the calculated first-order microscopic polarizability and described as the interaction between a selected dimer and the surrounding molecules in the bulk. Furthermore, the TPA coefficient β (in units of $cm\,GW^{-1}$) of a bulk material is determined by $\beta = N\delta/h\omega$.[36,37] Here N is again the dimer number density of the TPA compound (in units of cm^{-3}), δ the dimer TPA cross section of the same compound (in units of $cm^4 s^{-1}$ photon^{-1}), and $h\omega$ is excitation photon energy. Table 3 lists the calculated third-order susceptibilities of the DFWM process at an input energy of 1.165 eV and the TPA coefficients at resonant wavelength for the bulk materials of dimer-1 and dimer-2. It was found that the third-order susceptibilities and two-photon absorption coefficients of bulk materials are determined by those of corresponding dimers, and the bulk material constructed from dimer-2 has larger susceptibilities and two-photon absorption coefficients.

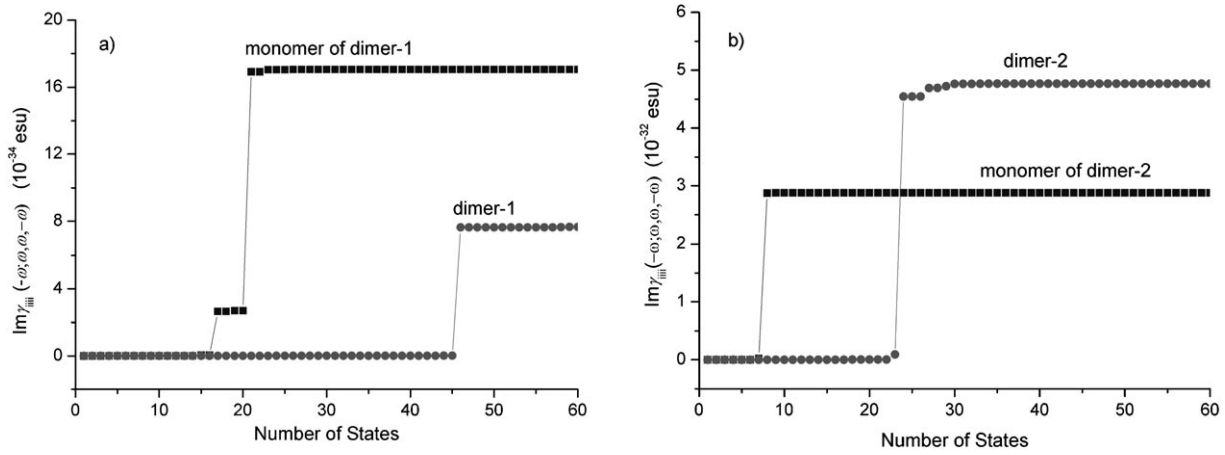

Figure 7. Plots of Im$\gamma(-\omega;\omega,\omega,-\omega)$ values versus two-photon states at the characteristic wavelength.

Table 3. Calculated third-order susceptibilities and two-photon absorption coefficients of bulk solids constructed from dimers.

Dimer	N [10^{21} cm^{-3}]	F	$\langle\gamma(\omega)\rangle$ [10^{-35} esu]	$\chi^{(3)}(\omega)$ [10^{-14} esu]	$\delta(\omega)$ [10^{-48} cm^4 s^{-1} photon^{-1}]	$\beta(\omega)$ [cm GW^{-1}]
1	1.253	1.1825	1.0645	1.577	0.249	0.801
2	0.6609	1.0942	210.09	151.9	4.630	12.03

Conclusion

Our DFT study showed that the oxime–oxime O–H···N bond energies are −9.636 and −8.551 kcal mol^{-1} for dimer-1 with simple pyridine oxime ligands and dimer-2 with extended pyridine oxime ligands, respectively, and that supramolecular structures based on oxime–oxime interactions are not substantially disrupted in spite of the enhanced dipole moment due to the extended pyridine oxime ligands of dimer-2. The lowest energy absorption band is red-shifted for dimer-2 compared with dimer-1, and the red shift is due to the fact that elongated (pyridylmethylene) aminoacetophenone oxime ligands lead to a significant increase in π–π delocalization interactions in dimer-2, while the hydrogen-bonding interactions are weaker in dimer-2 than in dimer-1. Charge transfer from π–π* orbitals of pyridine oxime ligands make significant contributions to the electronic absorption, third-order polarizabilities, and two-photon absorption cross sections for the monomers and dimers of $C_{12}H_{12}N_4O_2AgPF_6$ and $C_{28}H_{28}N_6O_3AgPF_6$. A *cis* arrangement of the two oxime moieties in the monomer results in an up-down wavy mode of connection in dimer-1, and this configuration results in small dipole moments, third-order polarizabilities, and two-photon absorption cross sections. A *trans* arrangement of the two oxime moieties in the monomer leads to head-to-tail mode of connection in dimer-2, and the resulting ladder configuration results in large dipole moments, third-order polarizabilities, and two-photon absorption cross sections. The optical properties of bulk materials are determined by those of the corresponding dimers. Dimer-2 has larger third-order polarizabilities and two-photon absorption cross sections, and the bulk material constructed from dimer-2 also has larger third-order susceptibilities and two-photon absorption coefficients.

Acknowledgements

This investigation was based on work supported by the National Natural Science Foundation of China under projects 20373073 and 90201015, the National Basic Research Program of China No.2004CB720605, the Science Foundation of the Fujian Province (E0210028), and the Foundation of State Key Laboratory of Structural Chemistry (030060).

[1] L. Brammer, *Chem. Soc. Rev.* **2004**, *33*, 476.
[2] P. Hubberstey, U. Suksangpanya, *Struct. Bonding (Berlin)* **2004**, *111*, 33.
[3] S. Kitagawa, R. Kitaura, S.-I. Noro, *Angew. Chem.* **2004**, *116*, 2388; *Angew. Chem. Int. Ed.* **2004**, *43*, 2334.
[4] A. M. Beatty, *Coord. Chem. Rev.* **2003**, *246*, 131.
[5] O. R. Eavans, W. Lin, *Acc. Chem. Res.* **2002**, *35*, 511.
[6] C. B. Aakeröy, A. M. Beatty, B. A. Helfrich, *Angew. Chem.* **2001**, *113*, 3340; *Angew. Chem. Int. Ed.* **2001**, *40*, 3240.
[7] *Crystal Engineering: From Molecules and Crystals to Materials, Vol. 538*, (Eds.: D. Braga, F. Grepioni, A. G. Orpen), NATO Science Series, Kluwer, Dordrecht, **1999**.
[8] G. S. He, J. D. Bhawalkar, C.-F. Zhao, P. N. Prasad, *Appl. Phys. Lett.* **1995**, *67*, 2433.
[9] J. E. Ehrlich, X. L. Wu, S. I.-Y. Lee, Z.-Y. Hu, H. Röckel, S. R. Marder, J. W. Perry, *Opt. Lett.* **1997**, *22*, 1843.
[10] D. R. Larson, W. R. Zipfel, R. M. Williams, S. W. Clark, M. P. Bruchez, F. W. Wise, W. W. Webb, *Science* **2003**, *300*, 1434.
[11] W. Denk, J. H. Strickler, W. W. Webb, *Science* **1990**, *248*, 73.
[12] C. Xu, W. Zipfel, J. B. Shear, R. M. Williams, W. W. Webb, *Proc. Natl. Acad. Sci. USA* **1996**, *93*, 10763.
[13] D. A. Parthenopoulos, P. M. Rentzepis, *Science* **1989**, *245*, 843.
[14] K. D. Belfield, K. J. Schafer, *Chem. Mater.* **2002**, *14*, 3656.
[15] C. B. Aakeröy, A. M. Beatty, D. S. Leinen, K. R. Lorimer, *Chem. Commun.* **2000**, 935.
[16] C. B. Aakeröy, A. M. Beatty, D. S. Leinen, *Angew. Chem.* **1999**, *111*, 1932; *Angew. Chem. Int. Ed.* **1999**, *38*, 1815.
[17] C. B. Aakeröy, A. M. Beatty, D. S. Leinen, *CrystEngComm* **2002**, *4*, 310.
[18] C. B. Aakeröy, A. M. Beatty, D. S. Leinen, *J. Am. Chem. Soc.* **1998**, *120*, 7383.
[19] A. D. Becke, *J. Chem. Phys.* **1993**, *98*, 5648.
[20] M. E. Casida, C. Jamorski, K. C. Casida, D. R. Salahub, *J. Chem. Phys.* **1988**, *180*, 4439.
[21] R. Bauernschmitt, R. Ahlrichs, *Chem. Phys. Lett.* **1996**, *256*, 454.
[22] R. E. Stratman, G. E. Scuseria, M. J. Frisch, *J. Chem. Phys.* **1998**, *109*, 8218.
[23] Gaussian 03, Revision C02, M. J. Frisch, G. W. Trucks, H. B. Schlegel, G. E. Scuseria, M. A. Robb, J. R. Cheeseman, J. A. Montgomery, Jr., T. Vreven, K. N. Kudin, J. C. Burant, J. M. Millam, S. S. Iyengar, J. Tomasi, V. Barone, B. Mennucci, M. Cossi, G. Scalmani, N. Rega, G. A. Petersson, H. Nakatsuji, M. Hada, M. Ehara, K. Toyota, R. Fukuda, J. Hasegawa, M. Ishida, T. Nakajima, Y. Honda, O. Kitao, H. Nakai, M. Klene, X. Li, J. E. Knox, H. P. Hratchian, J. B. Cross, C. Adamo, J. Jaramillo, R. Gomperts, R. E. Stratmann, O. Yazyev, A. J. Austin, R. Cammi, C. Pomelli, J. W. Ochterski, P. Y. Ayala, K. Morokuma, G. A. Voth, P. Salvador, J. J. Dannenberg, V. G. Zakrzewski, S. Dapprich, A. D. Daniels, M. C. Strain, O. Farkas, D. K. Malick, A. D. Rabuck, K. Raghavachari, J. B. Foresman, J. V. Ortiz, Q. Cui, A. G. Baboul, S. Clifford, J. Cioslowski, B. B. Stefanov, G. Liu, A. Liashenko, P. Piskorz, I. Komaromi, R. L. Martin, D. J. Fox, T. Keith, M. A. Al-Laham, C. Y. Peng, A. Nanayakkara, M. Challacombe, P. M. W. Gill, B. Johnson, W. Chen, M. W. Wong, C. Gonzalez, J. A. Pople, Gaussian, Inc., Pittsburgh, PA, **2003**.
[24] G. Maroulis, D. Xenides, U. Hohm, A. Loose, *J. Chem. Phys.* **2001**, *115*, 7957.
[25] T. R. Cundari, H. A. Kurtz, T. Zhou, *J. Phys. Chem. A* **1998**, *102*, 2962.
[26] W.-D. Cheng, D.-S. Wu, H. Zhang, X.-D. Li, D.-G. Chen, Y.-Z. Lang, Y.-C. Zhang, Y.-J. Gong, *J. Phys. Chem. B* **2004**, *108*, 12658.
[27] D.-S. Wu, W.-D. Cheng, H. Zhang, X.-D. Li, Y.-Z. Lan, D.-G. Chen, Y.-J. Gong, Y.-C. Zhang, *Phys. Rev. B* **2003**, *68*, 125402.
[28] D.-S. Wu, W.-D. Cheng, X.-D. Li, Y.-Z. Lan, D.-G. Chen, Y.-C. Zhang, H. Zhang, Y.-J. Gong, *J. Phys. Chem. A* **2004**, *108*, 1837.
[29] J. F. Ward, *Rev. Mod. Phys.* **1965**, *37*, 1.
[30] B. J. Orr, J. F. Ward, *Mol. Phys.* **1971**, *20*, 513.
[31] Two-photon absorption cross section $\delta(\omega)=(32\pi^4\hbar/n^2\lambda^2)L^4\mathrm{Im}\gamma[-\omega;\omega,\omega,-\omega]$, where n is the refractive index of of the medium (vacuum assumed for calculations) and L is a local field factor ($L=1$ for vacuum).

[32] X.-D. Li, W.-D. Cheng, D.-S. Wu, Y.-Z. Lan, H. Zhang, Y.-J. Gong, F.-F. Li, J. Shen, *J. Phys. Chem. B* **2005**, *109*, 5574.
[33] W.-D. Cheng, D.-S. Wu, X.-D. Li, Y.-Z. Lan, H. Zhang, D.-G. Chen, Y.-J. Gong, Y.-C. Zhang, F.-F. Li, J. Shen, Z.-G. Kan, *Phys. Rev. B* **2004**, *70*, 155401.
[34] The contribution to third-order polarizability from an individual state is calculated by the formula $x/\% = \Sigma_i(\gamma_i - \gamma_{i-1}]/\gamma_{conv}$.
[35] R. W. Boyd, *Nonlinear Optics*, Academic, San Diego, CA, **1992**, p. 148,.
[36] G. S. He, G. C. Xu, P. N. Prasad, B. A. Reinhardt, J. C. Bhatt, A. G. Dillard, *Optics Lett.* **1995**, *20[5]*, 435.
[37] P. L. Baldeck, Y. Morel, M. Plazanet, P. Feneyrou, C. Andraud, T. Brotin, C. Nguefack, A. Collet, J. F. Nicoud, A. Ibanez, "Optical Limiting Properties of Organic Nonlinear Crystals" in *Nonlinear Optical Properties of Organic Materials X* (Ed.: M. G. Kuzyk, Editor), *Proc. SPIE* **1997**, *3147*, 3147

Received: August 16, 2006
Revised: January 9, 2007
Published online: March 23, 2007

